Surface electron states on the quasi-two-dimensional excess-electron compounds Ca_{2}N and Y_{2}C

Takeshi Inoshita, Seiji Takemoto, Tomofumi Tada, and Hideo Hosono

Phys. Rev. B **95**, 165430 — Published 19 April 2017

DOI: 10.1103/PhysRevB.95.165430

Surface electron states on quasi-two-dimensional excess-electron compounds Ca_2N and Y_2C

Takeshi Inoshita,[1,2] Seiji Takemoto,[1] Tomofumi Tada,[1] and Hideo Hosono[1]

[1] *Materials and Structures Laboratory, Tokyo Institute of Technology, Nagatsuta, Kanagawa 226-8503, Japan*

[2] *National Institute for Materials Science, Tsukuba, Ibaraki 305-0044, Japan*

(Dated: February 9, 2017)

Abstract

Compounds having excess electrons from the formal valence viewpoint (electrides) are a new class of materials, which often take low-dimensional structures. We studied the (001) surface electronic structures of quasi-two-dimensional electrides Ca_2N and Y_2C by density functional theory using a slab model. Both materials were found to have a clean surface state well separated in energy from the bulk states. Furthermore, this state virtually floats above the surface and may be considered to be a hallmark of two-dimensional electrides. For Ca_2N, a tight-binding model in the Wannier representation was derived and analyzed, from which we concluded that the surface state, described by extra-surface s-like orbitals, is a Tamm state originating from an abrupt increase in potential energy at the surface.

I. INTRODUCTION

For more than half a century, layered materials with quasi-two-dimensional (Q2D) electronic structures have been a fertile ground of solid state physics and have led to the discovery of significant phenomena and concepts.[1,2] Archetypal Q2D materials include graphite and its intercalation compounds,[3] transition metal dichalcogenides,[4] cuprate and ion-based superconductors,[5–7] and various layered semiconductors (III-VI, IV-VI, hexagonal BN, etc.).[8] These materials have recently been receiving increased attention since many of them can be made atomically thin to realize ultimate two-dimensional (2D) materials.[9,10] In view of the significance of Q2D materials in both basic science and applications, an extensive search for new Q2D materials has been going on.

Layered dicalcium nitride Ca_2N is a unique material that emerged from such efforts. In 2013, Lee *et al.* found, through a combined experimental-computational study, that the material has a Q2D electronic structure[11] and, more importantly, that it is the first Q2D member to be classified in the category of unconventional materials named electrides.[12–14] This finding prompted a search for further Q2D electrides by ab initio calculations, resulting in the discovery of eight such materials in addition to Ca_2N.[15–17]

Electrides are ionic crystals in which electrons act as anions, i.e., electrons occupy sites that are normally occupied by anions.[12,13] Electrides contain more electrons than anticipated from the standard rules of valency (oxidation number), and these excess electrons are trapped around the interstitial sites, similarly to the way electrons occupy anion vacancies in alkali halides (color centers or F centers). A difference, however, is that electrides are regular stoichiometric compounds in which the density of the anionic electrons is periodic, unlike color centers which are random defects. For many years before the discovery of 2D electrides, the known electrides were either zero-dimensional (electrons confined in a cage) or one-dimensional (electrons confined in filamentary channels).[18,19]

The Q2D electrides known at present are three alkaline-earth nitrides AE_2N (AE=Ca, Sr, Ba) and six rare earth carbides (Y_2C and the $4f$ lanthanide carbides Ln_2C where Ln=Gd, Tb, Dy, Ho, Er).[16,17] (These do not include electrides that have been predicted to exist but have not yet been synthesized.[17]) We previously investigated their electronic structures by ab initio calculations, and have shown that the three nitrides are nonmagnetic metals, whereas the five lanthanide carbides are strongly ferromagnetic metals.[16]

In the case of Y_2C, density functional calculations indicate a weakly ferromagnetic ground state,[20] but an experiment conducted on polycrystalline samples showed no sign of ferromagnetism down to a temperature of 2 K.[21] (The measured magnetic susceptibility, however, has a peculiar temperature dependence.) Thus, Y_2C is believed to be close to the border between magnetic and nonmagnetic. On which side of the line it is located is yet to be determined.

Since Q2D electrides are unconventional materials with *anionic* electrons unassociated with any of the atoms, it should be interesting, from the perspectives of both fundamental research and applications (electronics,[11] catalysis,[22,23] etc.), to elucidate the nature of their surfaces. The present article investigates the surface electronic structures of prototypical Q2D electrides, Ca_2N and Y_2C, by density functional theory (DFT). For Y_2C, we neglect spin polarization because its ferromagnetism is expected to be weak, taking place only at very low temperatures.

The paper is organized as follows. Section II describes the crystal structures and the method of calculation. After a brief explanation of the electronic structures of bulk Ca_2N and Y_2C in Sec. IIIA, we present in Sec. IIIB the electronic structures of the (001) surfaces obtained by using DFT and a slab model. For Ca_2N, the DFT result is used in Section IV to derive and analyze a tight-binding model in the Wannier representation.

II. CRYSTAL STRUCTURE AND CALCULATION METHOD

As shown in Fig. 1, Ca_2N and Y_2C crystallize in the same anti-$CdCl_2$ structure (rhombohedral, space group $R\bar{3}m$) with a primitive unit cell containing three atoms (two Ca/Y atoms and one N/C atom at Wyckoff positions c and a, respectively).[24,25] The conventional unit cell is hexagonal with a volume three times larger than that of the primitive unit cell and contains nine atomic layers, forming the same (but staggered) triangular lattice. The nine layers can be grouped into three layer units (LUs), each made of three layers (Ca/N/Ca and Y/C/Y) stacked with a small distance of d =1.23 Å (Ca_2N) or 1.34 Å (Y_2C) separating the layers. The gap between these LUs, D, is much larger (3.81 Å and 3.30 Å for Ca_2N and Y_2C, respectively); it is this large gap that accommodates anionic (excess) electrons. Using the standard oxidation numbers of Ca, N, Y and C (+2, -3, +3 and -4, respectively), the charge arrangement in the c direction can be written schematically as $[CaNCa]^+ \cdot e^- \cdot [CaNCa]^+ \cdot e^- \cdot$

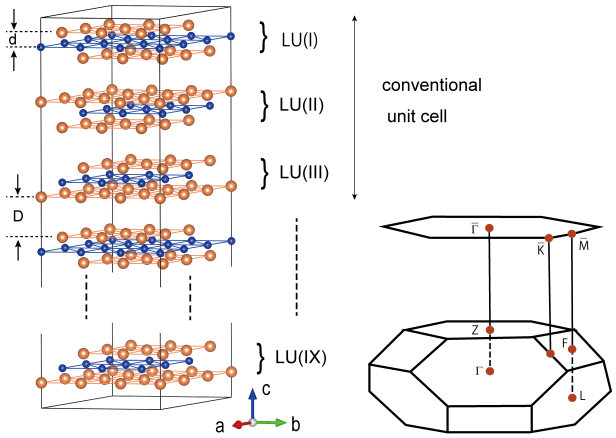

FIG. 1. Left panel: Crystal structure of Ca_2N and Y_2C (rhombohedral, $R\bar{3}m$), with the cations (metal) and anions shown by large orange spheres and small blue spheres, respectively. A conventional unit cell contains three layer units (LUs) arranged in ABC stacking [LU(I), LU(II), and LU(III)]. For ease of display, a supercell comprising $3 \times 3 \times 3$ conventional cells is drawn. The slab used for our surface calculation is a $1 \times 1 \times 3$ supercell, i.e., its height is the same as in this illustration but the lateral size is scaled by a factor of 1/3 in the a and b directions. Right panel: Bulk and (001) surface Brillouin zones.

$[CaNCa]^+$.... and $[YCY]^{2+}\cdot 2e^-\cdot[YCY]^{2+}\cdot 2e^-\cdot\ [YCY]^{2+}$...., where e^- denotes an excess electron occupying the inter-LU space. Note that Ca_2N has one excess electron per primitive unit cell, whereas Y_2C has two.

In the next section, we present the results of our DFT electronic structure calculation for the bulk and (001) slabs of Ca_2N and Y_2C. The calculations were carried out using the Vienna Ab initio Simulation Package (VASP)[26,27] employing a plane-wave basis set and projector augmented wave potentials.[28,29] The exchange-correlation energy was evaluated in the generalized gradient approximation proposed by Perdew, Burke and Ernzerhof (PBE).[30] The plane waves were cut off at 700 eV (600 eV) for the bulk (slabs), and the structures were relaxed until the forces on the atoms became smaller than 0.003 eV/Å (0.01 eV/Å) for the bulk (slabs). The k sampling mesh for Brillouin zone integration was chosen to be $11 \times 11 \times 11$ for the bulk and $13 \times 13 \times 1$ for the slabs, both centered at Γ.

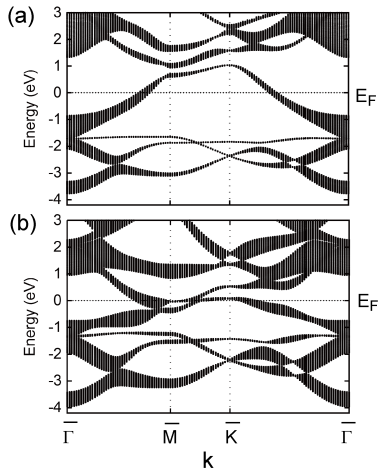

FIG. 2. Electronic band structure (Kohn-Sham energies plotted against 2D wavenumber $\boldsymbol{k}$) of bulk (a) Ca_2N and (b) Y_2C calculated by DFT projected onto the (001) surface Brillouin zone (right panel in Fig. 1).

III. ELECTRONIC STRUCTURE CALCULATION BY DFT

A. Bulk

With one excess electron per primitive unit cell, Ca_2N is expected to be a metal with a half-filled conduction band if there is no band overlap at the Fermi level. Our DFT calculation has confirmed this.[16] Figure 2(a) shows the energy band structure of Ca_2N projected onto the 2D surface Brillouin zone (hexagonal) illustrated in the right panel of Fig. 1. The Kohn-Sham energies of the Bloch electrons in the bulk are indicated by shaded areas. Here, the bands lying between -3.8 and -1.7 eV are essentially nitrogen p bands, whereas the band between -1.7 and 1 eV can be characterized as a half-filled anionic band. (Throughout the present paper, the Fermi energy E_F is set to zero.) The anionic band, which is the only band crossing E_F, has a charge density well confined between the LUs and has the nature of a 2D interlayer band. The bands lying above 1 eV are hybrid bands with a mixed Ca d-anionic electron character.

By similar reasoning, one would expect Y_2C, having two anionic electrons per primitive unit cell, to be a band insulator with a completely filled conduction band. This is not the case, as can be seen from its projected band structure [Fig. 2(b)]. The overlap between the first conduction band (anionic band) and the second conduction band (hybrid anionic-metal

band) makes Y_2C a semimetal having both electrons and holes. The charge density of the electrons at E_F is mainly confined in the gaps between the LUs but also penetrates further into the metal layers than in the case of Ca_2N.[16] This hybridization together with the strong Bragg reflection near the Brillouin zone boundary makes the conduction electron mass of Y_2C heavier than that of Ca_2N.

The dispersion in the c direction of the anionic band of Ca_2N, as indicated by the vertical width of the shaded area in Fig. 2(a), is largest at the band bottom (Γ point, energy between -1.7 and -0.8 eV) and decreases as the energy increases. The enhanced width near Γ is due to hybridization of the anionic band with the low-lying nitrogen p states. In the case of Y_2C, the width initially decreases upon moving away from Γ, similarly to Ca_2N, but then starts to increase owing to hybridization with the metal states [Fig. 2(b)].

B. (001) Slabs

We investigated the (001) surface electronic structures of Ca_2N and Y_2C using slabs containing nine LUs with the same height as in Fig. 1 but scaled by a factor of 1/3 in the a and b directions. A periodic stack of these slabs, with a gap of 30 Å between the layers, allows the system to be treated with plane waves. Starting from the bulk structure optimized in the previous section, the three LUs at both ends of the slab were relaxed while keeping the central three LUs frozen.

Figure 3(a) shows the calculated energy band structure of the Ca_2N slab. Surface bands may be identified by comparing this plot with Fig. 2(a) and noting that surface states, exponentially localized near the surface, can exist only in the gap regions [white areas in Fig. 2(a)] outside the bulk continua. Limiting ourselves to the bands traversing E_F, which are our interest, we can readily recognize a surface band (red points) located above the continuum of the bulk anionic band. Close scrutiny revealed that there is another surface band (blue points) located slightly below the continuum.[31] The close similarity in the shape of these surface bands to that of the bulk anionic band suggests that they are of the same anionic origin. In addition to the anionic surface bands, there are also surface bands derived from the nitrogen p states. These bands, highlighted in green in Fig. 3(a), will be briefly discussed in Sec. IV.[32]

The red solid line in Fig. 4(a) shows the layer-averaged partial electron density (PED) for

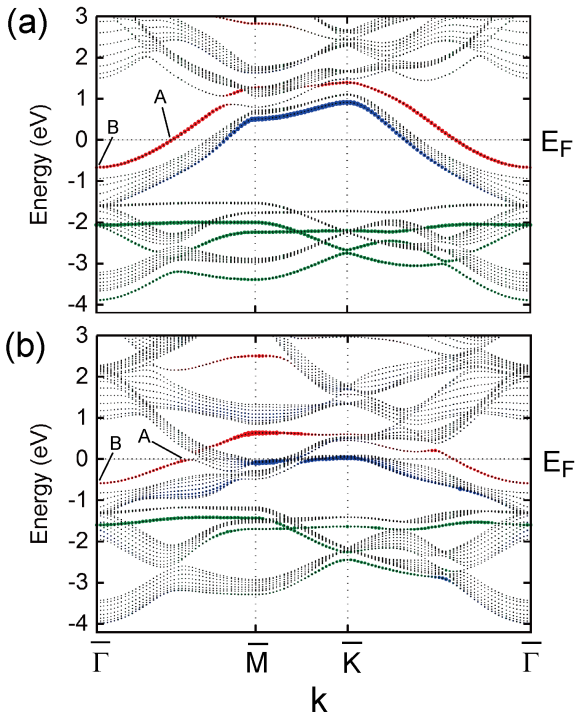

FIG. 3. Electronic band structures calculated by DFT for the nine-LU (001) slabs of (a) Ca_2N and (b) Y_2C (black points). Superimposed on these points are (i) blue dots whose radii indicate the probability of the electron being in the LU(I)-LU(II) gap and (ii) red dots, the radii of which are proportional to the probability of the electron being immediately outside the surface. At lower energies, the surface bands derived from nitrogen p states are highlighted in green.[32]

the energy range between -0.1 and 0 eV ($=E_F$). Also plotted by the black dashed line is the total valence electron density (VED), whose peaks indicate the positions of the ionic layers. As expected, the PED is mostly localized and accumulates in the inter-LU gaps with little penetration into the ionic layers. This reflects the inter-LU anionic character of the bands near E_F. More interesting is the similar accumulation of the PED outside the surfaces in both Ca_2N and Y_2C [indicated by asterisks in Figs. 4(a) and (c)]. To clarify the origin of this extra-surface electron accumulation, we calculate at each point (k, n) in Fig. 3(a) (k and n are the crystal momentum and band index, respectively) the probabillity that the electron occupies the gap between LU(I) and LU(II) (see Fig. 1). The radii of the blue dots in Fig. 3(a) indicate this probability. Similarly, the radii of the red dots in Fig. 3(a) denote the probability of the electron being immediately outside the surface. (Further explanation of how we evaluated the probability is given in the caption to Fig. 6.) The plot shows that

the above-continuum surface band is an anionic band localized *outside* the surface and is the origin of the extra-surface accumulation of electrons in Fig. 4(a). This conclusion is supported further by Fig. 4(b) which plots the PEDs for the above-continuum bands at k points A and B in Fig. 3(a). Similarly, the below-continuum surface band is an anionic band localized in the LU(I)-LU(II) gap. The charge distribution for this band is already bulklike, as can be seen from the similarity of the PED peak in the LU(I)-LU(II) gap to the corresponding peaks at the center of the slab. Note that the red and blue dots each occur on a single distinct branch of a band, indicating that their mutual hybridization as well as their hybridization with bulk states is very small, except at energies of more than 1 eV above E_F. In short, the (001) surface of Ca_2N has a clean extra-surface state at E_F, separated in energy and space from other states. It may therefore be worthwhile to study this surface as a high-mobility 2D electron system.

A similar feature, namely, the occurrence of two surface states, one outside the surface and the other in the LU(I)-LU(II) gap, can be seen on the surface of Y_2C as shown in Figs. 3(b), 4(c) and (d). A difference from Ca_2N, however, is that the density of the extra-surface electrons is smaller than that of the anionic electrons in the bulk, part of the density being pulled into the crystal [Figs. 4(c) and (d)]. This reduced exposure of the surface electrons to the environment may suppress, for example, the catalytic activity of Y_2C compared with that of Ca_2N.

Figure 5 shows the electron density contours in the [100] plane for the (001) slabs of Ca_2N and Y_2C. For each material, the VED is plotted on the left, while the PED for energies between -0.1 and 0 eV is presented on the right. As a result of the ABC stacking sequence in the bulk, all the densities in these slabs are quasi-periodic in the c direction with a period of three layers, i.e., LU(I) is similar to LU(IV), LU(II) is similar to LU(V) and so forth. Upon approaching the surface from the inside, the VEDs of both materials are practically unchanged as can be seen from Figs. 5(a) and (c). Changes from the bulk occur only outside the surfaces, where the VED decays more rapidly, and in the LU(I)-LU(II) gap, where the VED is slightly larger than in the gaps deeper inside. The PED for Ca_2N [Fig. 5(b)] clearly shows a flat sheet of electrons, corresponding to the extra-surface state, that accumulate above the outermost metal layer. This sheet is much thinner and flatter than its bulk counterpart in the LU(III)-LU(IV) gap. For the PED of Y_2C [Fig. 5(d)], the extra-surface state is not as clearly visible as that in Ca_2N owing to its lower density and

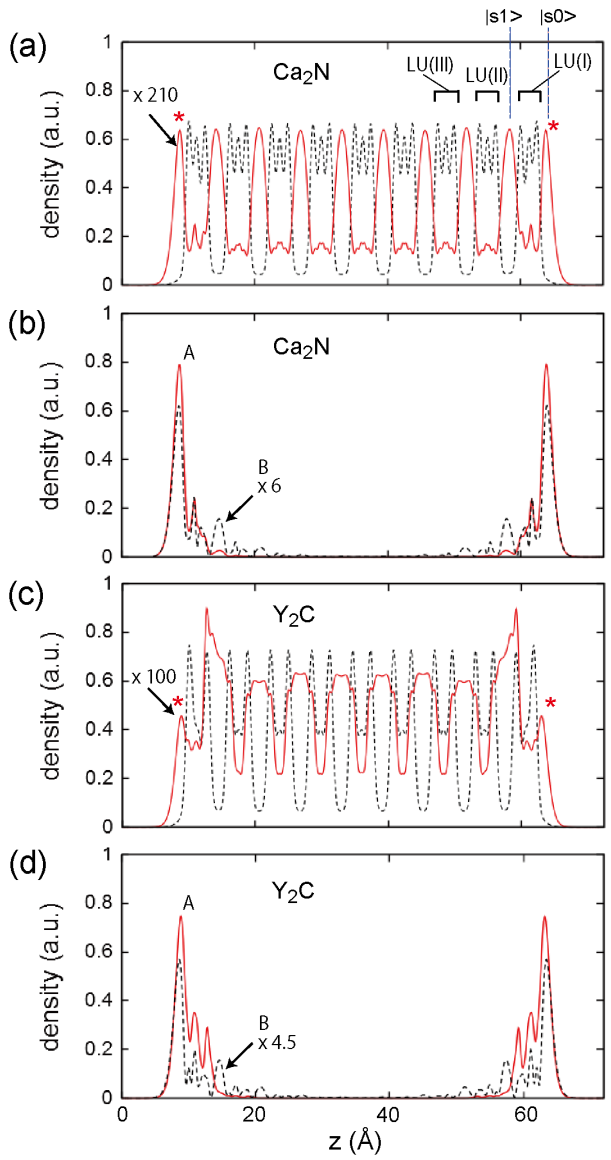

FIG. 4. (a) and (c): Layer-averaged PED for energy range -0.1 to 0 eV (red solid line) and total VED (black dashed line) calculated for the Ca_2N and Y_2C slabs, respectively. The peaks arising from the extra-surface states are indicated by asterisks. In (a), the positions of the centers of the Wannier orbitals $|s0\rangle$ and $|s1\rangle$ are indicated in the upper right. (b) and (d): Layer-averaged PEDs at k points A (red solid line) and B (black dashed line) in Figs. 3 for Ca_2N and Y_2C slabs, respectively.

larger spread in the c direction. The anionic electrons in the LU(I)-LU(II) gap have a higher density than those in the LU(IV)-LU(V) gap, in agreement with Fig. 4(c).

The distances between the metal layers after relaxation are shown in Fig. 6. In both

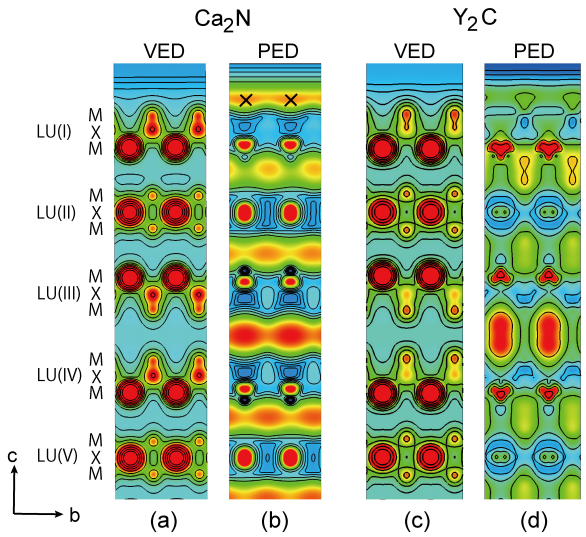

FIG. 5. Electron density contours in the [100] plane for (001) slabs of Ca_2N and Y_2C. (a) VED and (b) PED for Ca_2N. (c) VED and (d) PED for Y_2C. The PEDs are calculated for the energy range -0.1 eV $< E <$ 0 eV. The symbols M and X denote a metal ion (Ca/Y) and an anion (N/C), respectively. The crosses at the top of Fig. 5(b) indicate the positions of the Wannier orbital $|s0\rangle$ obtained in Sec. IV. The densities on successive contours are in the ratio of $\sqrt{3}$.

Ca_2N and Y_2C, the LU(I)-LU(II) gap shrinks by $> 1\%$, which is a feature generally seen in metals. The thickness of the LUs changes little, suggesting the internal rigidity of the LUs, except for LU(I) of Y_2C, the thickness of which decreases by 0.9%. This shrinkage suggests that ion-ion bonding in LU(I) is enhanced in Y_2C but its precise origin is not clear.

The emergence of an extra-surface band in 2D electrides is understandable from charge-neutrality considerations. Consider a Ca_2N slab with m LUs and $m-1$ inter-LU gaps. Suppose the charge density in the crystal were unchanged from that of the bulk (i.e., the charges of a LU and an inter-LU gap remained at +1 and -1, respectively) and there were no electron accumulation outside the slab. Then the slab would have a total charge of +1 and the electric field in the slab would diverge with increasing thickness. This divergence can be avoided by adding a charge of -1/2 on both surfaces of the slab. A similar restoration of charge neutrality is known to take place in, for example, oxide superlattices.[33] This scenario also holds in Y_2C, but the yttrium ions are not fully ionized, resulting in fewer electrons accumulating in the extra-surface space.

The extra-surface band found above survives in the limit of decreasing slab thickness.

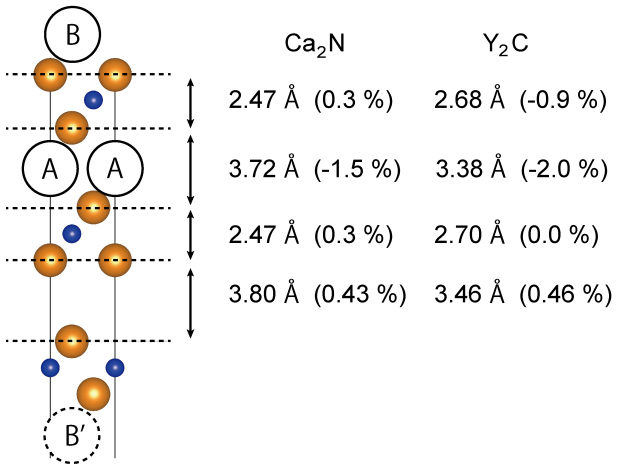

FIG. 6. Distances between near-surface metal layers in the relaxed slab. Their changes relative to the bulk values are shown in parentheses. The inter-LU probability, as indicated by the blue dots in Fig. 2, is calculated by integrating the square of the wave function, Ψ^2_{nk}, in a sphere of 1.3 Å radius at the interstitial position A. This position corresponds to the fractional coordinates (1/2, 1/2, 1/2) in the primitive unit cell [(0, 0, 0.5) in the conventional unit cell] in the bulk with Wyckoff position *b* and site symmetry $\bar{3}$m. Similarly, the extra-surface probability indicated by the red dots in Fig. 3 is obtained by placing a sphere of the same radius at an 'interstitial' position B of a hypothetical infinite crystal, which is equivalent to position B′.

As noted in Ref. 34, a single LU of Ca_2N holds *two* sheets of 2D electron gas, one above the LU and one below the LU [Fig. 7(a)]. These bands are split by tunnel coupling into bonding and antibonding bands and behave as a double quantum well. It is interesting to note that this splitting is rather large (1.0 eV) near the bottom of the bands (Γ point) owing to hybridization with nitrogen *p* bands but decreases with increasing energy (decreasing hybridization) to 0.4 eV near E_F. This small hybridization near E_F keeps the 2D electron system on Ca_2N detached from the ions, suggesting that it is less susceptible to perturbations such as phonons and disorder in the ionic layers. A similar double-quatum-well-like electronic structure can also be seen in Y_2C [Fig. 7(b)]. Compared with Ca_2N, the two quantum wells formed on the two sides of a single LU of Y_2C are coupled more strongly through hybridization with the ions. (We have confirmed the structural stability of a single LU of these materials by relaxation from a 3×3×1 supercell with slightly randomized atomic positions and lattice parameters.)

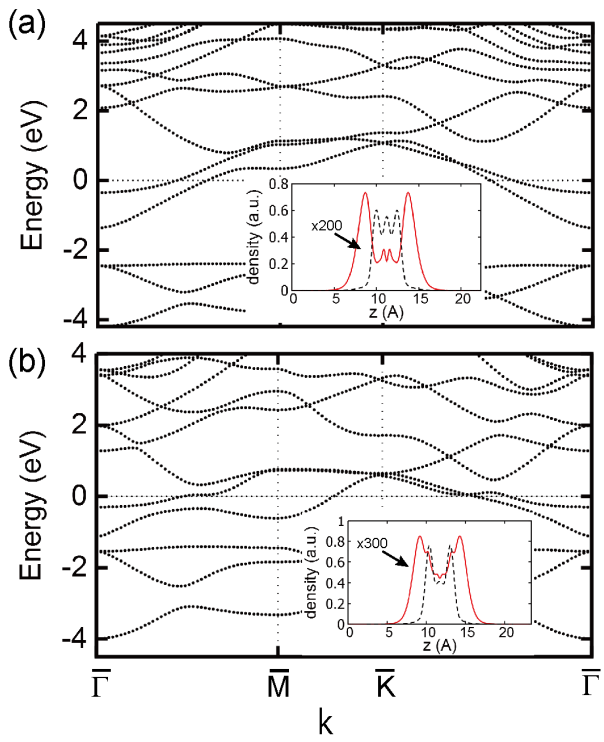

FIG. 7. Calculated band structure for a single LU of (a) Ca_2N and (b) Y_2C. The layer-averaged PED for energy -0.1 eV $< E <$ 0 eV (red solid line) and the total VED (black dotted line) are shown in the insets.

IV. WANNIER FUNCTION ANALYSIS OF Ca_2N (001) SURFACE

The nature and formation mechanism of surface states can be better understood by constructing a tight-binding model from the DFT electronic structure. A useful scheme for carrying out this transformation is the maximally localized Wannier function (MLWF) method.[35,36] The method not only allows the construction of a tight-binding basis (Wannier functions) and a Hamiltonian but also facilitates the analysis of chemical bonding. Wannier functions (WFs) are spatially localized orbitals derived by Fourier transforming linear combinations of Bloch functions.[37,38] WFs are not unique due to the arbitrariness in the phases of the Bloch functions. The MLWF method takes advantage of this phase freedom together with a unitary transformation to obtain WFs with the smallest spatial spread. The positions of the WFs are also optimized.

Following Ref. 39, let us write the WFs in a given unit cell as $|\mathbf{0}\alpha\rangle$, where α is an index specifying the WFs. These functions can be used to construct the Bloch sums

$$|\phi_{\alpha\boldsymbol{k}}\rangle = \frac{1}{\sqrt{N}} \sum_{\boldsymbol{R}} e^{i\boldsymbol{k}\cdot\boldsymbol{R}} |\boldsymbol{R}\alpha\rangle, \tag{1}$$

where $|\boldsymbol{R}\alpha\rangle$ is the WF $|\boldsymbol{0}\alpha\rangle$ shifted by a lattice vector $\boldsymbol{R}$, and N is the number of unit cells. The Hamiltonian of the system is diagonal in $\boldsymbol{k}$ and its Wannier representation is

$$H_{\boldsymbol{k},\alpha\beta} = \langle\phi_{\alpha\boldsymbol{k}}|H|\phi_{\beta\boldsymbol{k}}\rangle = \sum_{\boldsymbol{R}} e^{i\boldsymbol{k}\cdot\boldsymbol{R}} \langle\boldsymbol{0}\alpha|H|\boldsymbol{R}\beta\rangle. \tag{2}$$

Let us write the Bloch functions as linear combinations of $|\phi_{\alpha\boldsymbol{k}}\rangle$

$$|\Psi_{\boldsymbol{k}}\rangle = \sum_{\alpha} C_{\boldsymbol{k}\alpha} |\phi_{\alpha\boldsymbol{k}}\rangle, \tag{3}$$

where the coefficients are normalized as $\sum_\alpha C^2_{\boldsymbol{k}\alpha} = 1$. Inserting Eq. 3 into the Schrödinger equation $H|\Psi_{n\boldsymbol{k}}\rangle = E_{n\boldsymbol{k}}|\Psi_{n\boldsymbol{k}}\rangle$ and using the orthonormality of $\{|\boldsymbol{R}\alpha\rangle\}$, one arrives at the secular equation

$$\sum_{\beta} H_{\boldsymbol{k},\alpha\beta} C_{n\boldsymbol{k},\beta} = E_{n\boldsymbol{k}} C_{n\boldsymbol{k},\alpha}, \tag{4}$$

where the band index n is written explicitly. The solution of Eq. 4 provides an energy band structure that approximates the DFT band structure. We use the WANNIER90 code[40] to obtain $|0\alpha\rangle$ and $\langle\boldsymbol{0}\alpha|H|R\beta\rangle$ for the Ca_2N slab from the output of the DFT band calculation carried out in Sec. III [Fig. 3(a)]. A k mesh of 5×5×1 is used for the WF fitting. An energy window of -4 to 0.9 eV is employed to select the Bloch functions used in the Wannier transformation.

Figure 8 compares the energy bands obtained by DFT (black) and those obtained by the solution of Eq. 4 (red). The agreement can be seen to be very good from the valence bands up to at least 0.5 eV above E_F. The optimized WFs (Fig. 9) appear as three types: (i) eight s-like orbitals, one in the middle of each gap between the LUs, (ii) two s-like orbitals located outside the upper and lower surfaces, respectively, and (iii) 27 p-like (p_x, p_y, p_z) orbitals centered at nitrogen sites. The s-like orbitals (i) and (ii) clearly account for the anionic bands ranging between -1.6 and 1 eV, while orbitals (iii) describe the valence bands below -1.6 eV. In Fig. 8(b), the centers of the orbitals near the upper surface are indicated by crosses. The $|sm\rangle$ ($m = 1, 2, 3, \cdots, 8$) are type (i) orbitals in the mth inter-LU gap with their centers at the interstitial sites (symmetry $\bar{3}m$, Wyckoff symbol b) except for $|s1\rangle$,

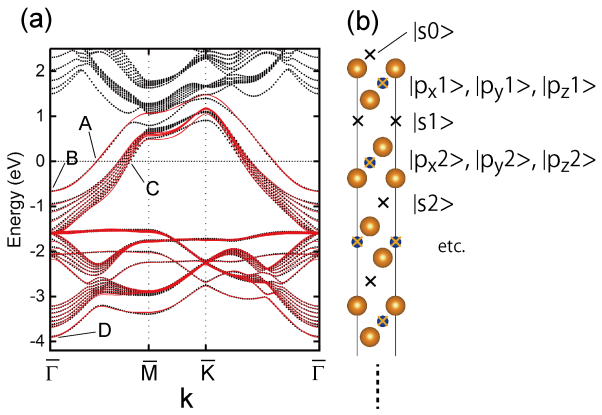

FIG. 8. (a) Energy band structure of the Ca_2N (001) slab. The black dots denote the result of a DFT calculation [same as Fig. 3(a)]. The red dots show the energy bands obtained by diagonalizing the tight-binding Hamiltonian with maximally localized WFs as the basis. (b) Positions of Wannier centers indicated by crosses. The large (orange) spheres and small (blue) spheres denote Ca and N atoms, respectively.

which is shifted slightly away from the b position towards the surface. $|s0\rangle$ is the type (ii) orbital at the top of the slab. It is the extra-surface counterpart of $|sm\rangle$ and has a similar shape and spatial spread to $|sm\rangle$. A difference is that $|s0\rangle$ is closer to the adjacent metal layer. (There is also a type (ii) orbital at the bottom of the slab but we do not refer to it in this article.) Finally, $|p_{x,y,z}m\rangle$ ($m = 1, 2, 3, \cdots, 9$) are type (iii) orbitals located at the nitrogen sites, even near the surface, indicating the rigidity of the LUs. The index m used to designate the WFs can be replaced by the z coordinates (denoted as Z) of their centers. This leads to an alternative indexing of the WFs as $|sZ\rangle$, $|p_xZ\rangle$, $|p_yZ\rangle$ and $|p_zZ\rangle$. We use both nomemclatures in the following.

Figure 10 shows the on-site energies $E_{\gamma Z} = \langle \mathbf{0}\gamma Z|H|\mathbf{0}\gamma Z\rangle$ as a function of Z where $\gamma = s, p_x, p_y, p_z$. For each γ, $E_{\gamma Z}$ is reasonably flat inside the crystal. The truncation of the crystal affects only up to two LUs below the surface. Upon approaching the surface from the inside, E_{sZ} (red circles) decreases slightly at $|s1\rangle$ and then increases abruptly by 0.9 eV outside the surface ($|s0\rangle$). The rise at the surface is consistent with the increase in potential energy generally observed outside crystal surfaces. The on-site energies for the p orbitals (E_{p_xZ}, E_{p_yZ}, E_{p_zZ}) show the opposite behavior to the s orbitals and decrease at the surface. This contrasting behavior may be required for preserving charge neutrality

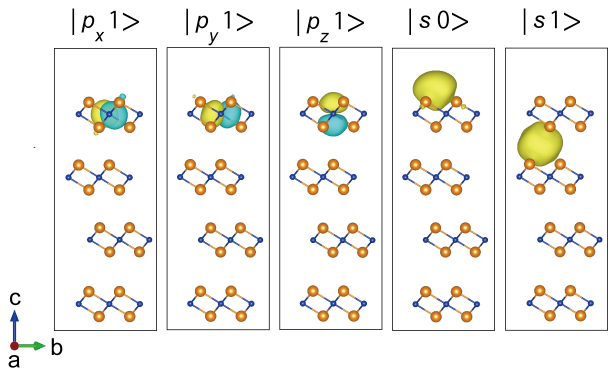

FIG. 9. Isosurface graphics of maximally localized WFs obtained. Only the functions located near the surface are shown. $|p_x1\rangle$, $|p_y1\rangle$, $|p_z1\rangle$: p-like WFs centered at the nitrogen site in LU(I). $|s0\rangle$: s-like WF outside the surface, $|s1\rangle$: s-like WF slightly off the interstitial site in the LU(I)-LU(II) gap.

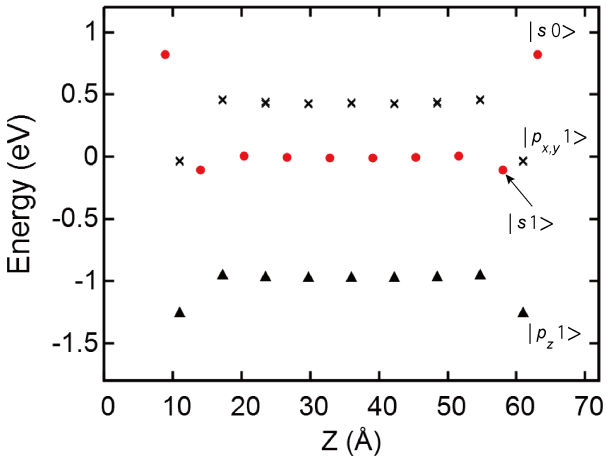

FIG. 10. On-site energies $E_{\gamma Z}$ of the Wannier orbitals (diagonal elements of the tight-binding Hamiltonian) plotted against the z coordinates of their centers. The s orbitals, $p_{x,y}$ orbitals and p_z orbitals are indicated by red circles, black crosses and black triangles, respectively.

in the crystal. A notable feature here is the large separation in energy between the $|s0\rangle$ and $|p_{x,y,z}1\rangle$ orbitals (the p_z orbital, in particular). This energy difference should be vital for suppressing the hybridization between these orbitals and keeping the extra-surface state clean and free-electron like.

The transfer integrals between the WFs (off-diagonal elements of the Hamiltonian $\langle \mathbf{0}\alpha|H|\boldsymbol{R}\beta\rangle$) are found to be reasonably small (< 0.35 eV). The interlayer s-s transfer is only 0.029 eV (0.019 eV) at the surface (in bulk), which is an order of magnitude smaller

than the interlayer s-p transfer of 0.22 to 0.30 eV (0.15 to 0.20 eV) at the surface (in the bulk). (The spread of these numbers is due to the fact that there are three p orbitals.) Therefore, the dispersion of the anionic bands in the c direction is dominated by the s-p transfers, not by the s-s transfers. The intralayer s-s transfer at the surface is 0.30 eV and is smaller than the bulk value of 0.34 eV, which is consistent with the smaller width of the surface band. The transfer integrals were found to be uniform across the thickness of the slab, deviating from the bulk value only at the outermost LU.

Since the interlayer transfer is dominated by s-p couplings, it is worthwhile to formally eliminate the p orbitals from Eq. 4 (which is a 37×37 matrix equation) and considering a 10 × 10 effective Hamiltonian spanned only by the s orbitals. This is achieved by separating the matrix $H_{\boldsymbol{k}}$ into s and p blocks and writing Eq. 4 as

$$\begin{pmatrix} H_{\boldsymbol{k}}^{ss} & H_{\boldsymbol{k}}^{sp} \\ H_{\boldsymbol{k}}^{ps} & H_{\boldsymbol{k}}^{pp} \end{pmatrix} \begin{pmatrix} C_{\boldsymbol{k}s} \\ C_{\boldsymbol{k}p} \end{pmatrix} = E_{\boldsymbol{k}} \begin{pmatrix} C_{\boldsymbol{k}s} \\ C_{\boldsymbol{k}p} \end{pmatrix}, \tag{5}$$

where $C_{\boldsymbol{k}s}$ and $C_{\boldsymbol{k}p}$ are column vectors and the band index is suppressed. Eliminating $C_{\boldsymbol{k}p}$ from Eq. 5, we obtain

$$\tilde{H}_{\boldsymbol{k}} C_{\boldsymbol{k}s} = E_{\boldsymbol{k}} C_{\boldsymbol{k}s}, \tag{6}$$

$$\tilde{H}_{\boldsymbol{k}} = H_{\boldsymbol{k}}^{ss} + H_{\boldsymbol{k}}^{sp} (E_{\boldsymbol{k}} - H_{\boldsymbol{k}}^{pp})^{-1} H_{\boldsymbol{k}}^{ps}. \tag{7}$$

Although Eq. 6 contains $E_{\boldsymbol{k}}$ on both sides, its similarity in form to a one-dimensional tight-binding equation is useful for analyzing our system. For example, setting $\boldsymbol{k}$ to 0 and $E_{\boldsymbol{k}}$ to the energy of the anionic band at Γ, the nearest-neighbor off-diagonal elements of $\tilde{H}_{\boldsymbol{k}=0}$ (s-s transfers mediated by the p orbitals) are all equal to 0.29 eV except at the surface, where they increase to 0.43 eV. The second-nearest-neighbor transfers are very small ($<$ 0.06 eV). The on-site (diagonal) elements behave in a similar manner to the red points in Fig. 10, increasing abruptly by 0.91 eV at the surface but otherwise remaining quite uniform. Overall, our system is well described by a truncated one-dimensional nearest-neighbor tight-binding model in which the on-site energy is larger at the surface than in the bulk.

A thorough discussion of this model is given in Ref. 41 using the semi-infinite tridiagonal Hamiltonian $\mathcal{H}_{ii} = \delta_{i0}\,\alpha' + (1 - \delta_{i0})\alpha$ and $\mathcal{H}_{i,i+1} = \mathcal{H}_{i+1,i} = \beta$ where $i = 0, 1, 2, 3 \cdots$. It is shown that if $v \equiv (\alpha' - \alpha)/|\beta| > 1$, there is a single surface state (called the "P state")

above the bulk continuum, while for $v < -1$ another surface state (called the "N state") appears *below* the bulk continuum. No surface state exists if $|v| \leq 1$. Also, the P state is more localized than the N state. Using the values of $\alpha' - \alpha$ and β obtained from our $\tilde{H}_{\boldsymbol{k}=0}$, v for the Ca_2N slab is estimated to be 2.8 (> 1), which explains the emergence of a surface state (P state) above the bulk continuum in our DFT result. A surface state caused by such an abrupt change in the potential (on-site energy) at the surface is called a Tamm state. Thus, the surface state that appears outside a Ca_2N surface is a textbook example of a Tamm state, similar to those found in semiconductor superlattices.[42]

Figure 11 shows a plot of $(C_{n\boldsymbol{k},\gamma Z})^2$, i.e., the weight of the γZ WF in the Bloch function expansion, at various n and $\boldsymbol{k}$ as a function of Z. The s orbitals, $p_{x,y}$ orbitals and p_z orbitals are shown by red circles, black crosses and black triangles, respectively. Figures 11(a) to (d) correspond to $(\boldsymbol{k}, n)$ at points A to D, respectively, in Fig. 8. It can be seen that state A almost entirely consists of the extra-surface s orbital ($|s0\rangle$) and its counterpart on the other surface. The contribution of other orbitals, even the subsurface s orbital ($|s1\rangle$) and p orbitals ($|p_{x,y,z}1\rangle$), is negligibly small. At the bottom (Γ point, indicated as B), the band is hybridized to some extent with the orbitals $|s1\rangle$ and $|p_{x,y,z}1\rangle$, but its extra-surface character remains. This strong localization of the extra-surface anionic band in the c direction, in agreement with the DFT results, is consistent with its interpretation as a P state. Also, its small hybridization with other orbitals suggests its clean free-electron-like nature. As can be seen from Fig. 11(c), state C, which is located slightly below the bulk continuum, is also a surface state consisting mainly of $|s1\rangle$, consistent with our discussion in Sec. III. The presence of this second surface state cannot be accounted for by the simple Hamiltonian $\mathcal{H}$. We ascribe it to the dip in the on-site energy of $|s1\rangle$ (the second red dot from the right in Fig. 10). Finally, as can be seen from Fig. 11(d), state D in Fig. 8 is a nitrogen p-like surface state localized on the nitrogen site in LU(I). It is somewhat hybridized with $|s0\rangle$ and $|s1\rangle$ but shows little hybridization with the inner p-like states. In spite of the complexity arising from the quasi-degeneracy of the p_x, p_y and p_z orbitals, the p bands are organized into three distinct groups separated in energy as can be seen from Fig. 2(a). Each of these groups is accompanied by a surface band located at a lower energy (Fig. 8). We interpret these surface bands as N bands arising from the decrease in the on-site energies at the surface shown in Fig. 10 (black crosses and triangles). The less localized character of these surface bands [Fig. 11(d)] is consistent with the general trait of the N surface state.[41]

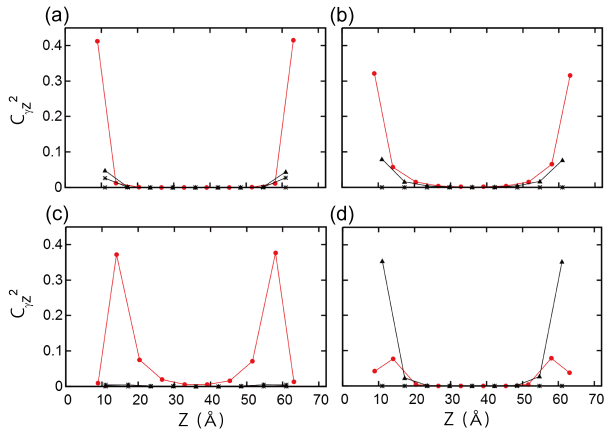

FIG. 11. Weight $C^2_{nk,\gamma Z}$ ($\gamma = s, p_x, p_y, p_z$) of WFs in the Bloch function expansion (Eq. 3) at various (k, n) plotted against the Wannier center coordinate Z. The s orbitals, $p_{x,y}$ orbitals and p_z orbitals are indicated by red circles, black crosses and black triangles, respectively. (a) to (d) correspond to (k, n) at points A to D, respectively, in Fig. 8.

V. CONCLUDING REMARKS

We have carried out DFT electronic structure calculations for nine LU (001) slabs of Ca_2N and Y_2C. The main findings are as follows. (1) Both compounds host clean extra-surface states, one on each surface, which are well separated in energy and space from the bulk states. These states are extra-surface analogs of the interlayer anionic states in the bulk. (2) For Ca_2N, the electronic structure of the slab can be well described by a tight-binding model in the Wannier representation. (3) An analysis of the tight-binding Hamiltonian revealed that the extra-surface state is a Tamm state originating from the abrupt increase in potential energy.

Some noble metals are known to have very clean surface states with a long coherence length, as demonstrated by the observation of a quantum mirage in quantum corrals formed on a Cu(111) surface.[43] Since the extra-surface electrons on (001) Ca_2N, and presumably those on other Q2D electrides with similar electronic structures such as Sr_2N, are free-electron-like and float above the surface, detached from the ions, they are expected to have a longer coherence/scattering length than those on ordinary metals. It would therefore be worthwhile to study the transport characteristics of the surface electrons on Q2D electrides and compare them with those of noble metals.

The extra-surface, spatially isolated electrons on a 2D electride can serve as activators

of chemical reactions with foreign atoms and/or molecules without seriously affecting the anionic electrons in the bulk. Hence, the chemical or physical tuning of the surface states may provide opportunities for the development of unconventional chemical reaction routes if the surface area is enhanced by an appropriate exfoliation procedure.

ACKNOWLEDGMENTS

T.I. would like to thank Drs. Masaru Tsukada and Susumu Saito for valuable discussions. This work was supported by the MEXT Elements Strategy Initiative to Form Core Research Center and the JST ACCEL Program. Crystal structure graphics were generated by VESTA.[44]

---

[1] *Crystallography and Crystal Chemistry of Materials with Layered Structures*, ed. F. Levy (D. Reidel, Dordrecht, 1976).

[2] *Electronic Structure and Electronic Transitions in Layered Materials*, ed. V. Grasso (D. Reidel, Dordrecht, 1986).

[3] T. Enoki, M. Suzuki, and M. Endo, *Graphite Intercalation Compounds and Applications* (Oxford University Press, New York, 2003).

[4] A. V. Kolobov and J. Tominaga, *Two-Dimensional Transition-Metal Dichalcogenides* (Springer International Publishing, Switzerland, 2016)

[5] N. Plakida, *High-Temperature Cuprate Superconductors: Experiment, Theory, and Applications* (Springer, Heidelberg, 2010).

[6] G. R. Stewart, Rev. Mod. Phys. **83**, 1589 (2011).

[7] H. Hosono and K. Kuroki, Physica C **514**, 399 (2015).

[8] O. Madelung, *Semiconductors: Data Handbook* (Springer-Verlag, Berlin, 2004).

[9] S. Lebègue, T. Björkman, M. Klintenberg, R. M. Nieminen, and O. Eriksson, Phys. Rev. X **3**, 031002 (2013).

[10] K. S. Novoselov, A. Mishchenko, A. Carvalho, and A. H. Castro Neto, Science **353**, aac9439 (2016).

[11] K. Lee, S. W. Kim, Y. Toda. S. Matsuishi, and H. Hosono, Nature **494**, 336 (2013).

[12] J. L. Dye, Science **247**, 663 (1990).

[13] J. L. Dye, Science **301**, 607 (2003).

[14] S. Matsuishi, Y. Toda, M. Miyakawa, K. Hayashi, T. Kamiya, M. Hirano, I. Tanaka, and H. Hosono, Science **301**, 626 (2003).

[15] A. Walsh and D. O. Scanlon, J. Mater. Chem. C **1**, 3525 (2013).

[16] T. Inoshita, S. Jeong, N. Hamada, and H. Hosono, Phys. Rev. X **4**, 031023 (2014).

[17] T. Tada, S. Takemoto, S. Matsuishi, and H. Hosono, Inorg. Chem. **53**, 10347 (2014).

[18] J. L. Dye, M. J. Wagner, G. Overney, R. H. Huang, T. F. Nagy, and D. Tománek, J. Am. Chem. Soc. **118**, 7329 (1996).

[19] Y. Zhang, Z. Xiao, T. Kamiya, and H. Hosono, J. Phys. Chem. Lett. **6**, 4966 (2015).

[20] T. Inoshita, N. Hamada, and H. Hosono, Phys. Rev. B **92**, 201109(R), 2015.

[21] X. Zhang, Z. Xiao, H. Lei, Y. Toda, S. Matsuishi, T. Kamiya, S. Ueda, and H. Hosono, Chem. Mater. **26**, 6638 (2014).

[22] Y. J. Kim, S. M. Kim, E. J. Cho, H. Hosono, J. W. Yang, and S. W. Kim, Chem. Sci. **6**, 3577 (2015).

[23] M. Kitano, Y. Inoue, H. Ishikawa, K. Yamagata, T. Nakao, T. Tada, S. Matsuishi, T. Yokoyama, M. Hara, and H. Hosono, Chem. Sci. **7**, 4036 (2016).

[24] E. T. Keve and A. C. Skapski, Inorg. Chem. **7**, 1757 (1968).

[25] M. Atoji and M. Kikuchi, J. Chem. Phys. **51**, 3863 (1969).

[26] G. Kresse and J. Furthmüller, Phys. Rev. B **54**, 11169 (1996).

[27] G. Kresse and J. Furthmüller, Comput. Mater. Sci. **6**, 15 (1996).

[28] P. E. Blöchl, Phys. Rev. B **50**, 17953 (1994).

[29] G. Kresse and D. Joubert, Phys. Rev. B **59**, 1758 (1999).

[30] J. P. Perdew, K. Burke, and M. Ernzerhof, Phys. Rev. Lett. **77**, 3865 (1996).

[31] What appears to be a single surface band in Figs. 3 and 8 actually consists of two quasi-degenerate bands, localized near the upper surface and lower surface, respectively. Their splitting due to the finite width of the slab is invisibly small, indicating that the surface states are well localized and the slabs are sufficiently thick.

[32] The radii of the green dots in Figs. 3 are proportional to the difference between the electron density in the surface N layer and that in the subsurface N layer and therefore indicate the degree of localization in the c direction.

[33] K. Yoshimatsu, R. Yasuhara, H. Kumigashira, and M. Oshima, Phys. Rev. Lett. **101**, 026802 (2008).

[34] S. Zhao, Z. Li, and J. Yang, J. Am. Chem. Soc. **136**, 13313 (2014).

[35] N. Marzari and D. Vanderbilt, Phys. Rev. B **56**, 12847 (1997).

[36] I. Souza, N. Marzari, and D. Vanderbilt, Phys. Rev. B **65**, 035109 (2001).

[37] G. H. Wannier, Phys. Rev. **52**, 191 (1937)

[38] W. Kohn, Phys. Rev. **115**, 809 (1959).

[39] N. Marzari, A. A. Mostofi, J. R. Yates, I. Souza, and D. Vanderbilt, Rev. Mod. Phys. **84**, 1419 (2012).

[40] A. A. Mostofi, J. R. Yates, Y.-S. Lee, I. Souza, D. Vanderbilt, and N. Marzari, Comput. Phys. Commun. **178**, 685 (2008).

[41] S. G. Davison and M. Stęślicka, *Basic Theory of Surface States* (Clarendon Press, Oxford, 1992), Chap. 4. The β in Eqs. (4.4) and (4.8) should be replaced by $|\beta|$.

[42] H. Ohno, E. E. Mendez, J. A. Brum, J. M. Hong, F. Agullo-Rueda, L. L. Chang, and L. Esaki, Phys. Rev. Lett. **64**, 2555 (1990).

[43] M. F. Crommie, C. P. Lutz, and D. M. Eigler, Science **262**, 218 (1993).

[44] K. Momma and F. Izumi, J. Appl. Crystallogr. **44**, 1272 (2011).